CHEMISTRY OF MATERIALS

Article

pubs.acs.org/cm

Synthesis, Structure, and Electrochemical Properties of the Layered Sodium Insertion Cathode Material: $NaNi^{1}_{/3}Mn^{1}_{/3}Co^{1}_{/3}O_2$

M. Sathiya,[†] K. Hemalatha,[†] K. Ramesha,[†] J.-M. Tarascon,[‡] and A. S. Prakash*,[†]

[†]CSIR Central Electrochemical Research Institute-Chennai Unit, CSIR-Madras Complex, Taramani, Chennai-600 113, India

[‡]Laboratoire de Réactivité et Chimie des Solides, CNRS UMR 7314, 33, rue Saint Leu - Université de Picardie Jules Verne, 80039 Amiens, France

Supporting Information

ABSTRACT: A layered phase, $NaNi^{1}_{/3}Mn^{1}_{/3}Co^{1}_{/3}O_2$ (NaNMC), isostructural to $NaCoO_2$ has been synthesized. Stoichiometric NaNMC crystallizes in a rhombohedral $R\bar{3}m$ space group where Na is in an octahedral environment (O3-Type). Galvanostatic cycling on NaNMC vs Na cell indicated a reversible intercalation of 0.5 Na, leading to a capacity of 120 mAh·g^{-1} in the voltage range of 2−3.75 V and indicating its possible application in Na-ion batteries. The electrochemically driven Na insertion/deinsertion in NaNMC is associated with several phase transitions and solid solution regimes which are studied by *in situ* X-ray diffraction. Sodium deinsertion in Na_xNMC resulted in sequential phase transitions composed of biphasic and monophasic domains. The composition driven structural evolution in Na_xNMC follows the sequence O3 ⇒ O1 ⇒ P3 ⇒ P1 phases with an increased '*c*' parameter, while the '*a*' parameter remains almost unchanged.

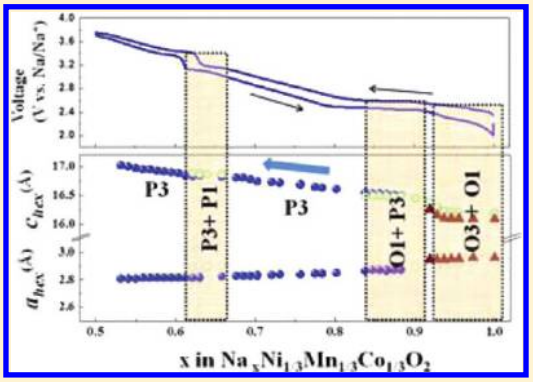

KEYWORDS: *sodium-ion batteries, layered compounds, NaNMC, in situ XRD*

INTRODUCTION

Lithium ion batteries have emerged as the best suited power source for portable electronics.[1,2] They are also being considered as strong contenders to meet the energy demands of the transport sector. However, there is a serious concern about the availability of lithium if electric vehicles become the reality of the future.[3] Under such circumstances finding an alternative to lithium is inevitable and is of utmost priority to develop sustainable secondary batteries.[4] Sodium is abundant, and its electropositive nature is closer to Li. Therefore, developing sodium secondary batteries offers attractive advantage in terms of cost, safety, and sustainability.[5]

Sodium, being bigger in size than lithium and also due to its larger screening effect, has a strong tendency to favor the formation of layered compounds. For instance, compounds of $NaMX_2$-type such as Na_xCoO_2, Na_xNiO_2, Na_xMnO_2, Na_xTiS_2, and Na_xTaS_2[6−11] form a layered structure. These compounds were shown to reversibly insert Na ions, however, with limited capacity and rate capability. To overcome these issues, efforts have been focused toward developing improved electrode materials for sodium ion batteries. Solid solutions of Na_xMO_2 phases such as $Na_xNi_{0.5}Mn_{0.5}O_2$, $Na_xNi_{1-y}Co_yO_2$, etc. are known to exhibit interesting electrochemical performance.[12,13] Komaba et al.[14] reported a stable capacity of 125 mAh·g^{-1} with the $Na_xNi_{0.5}Mn_{0.5}O_2$ phase when cycled in the voltage window of 2.5 to 3.5 V. They have also demonstrated that a high capacity of 185 mAh·g^{-1} could be tapped when cycled up to 4.8 V but with a huge capacity loss.

The lithium counterparts of the aforementioned phases have been intensively studied as insertion hosts vs Li, and among them the $LiNi^{1}_{/3}Mn^{1}_{/3}Co^{1}_{/3}O_2$[15] phase, commonly called LiNMC, is presently the stellar. LiNMC electrodes show a sustained reversible capacity of 200 mAh·g^{-1} vs Li[16] at a voltage greater than 4 V, which is mainly associated to the $Ni^{2+}⇔Ni^{4+}$ redox process. Owing to such performances, Li-ion cells based on positive electrodes are now widely commercialized. Within this context, the $NaNi_{1/3}Mn_{1/3}Co_{1/3}O_2$ phase, which is the sodium counterpart of the commercially exploited NaNMC phase, appears as an attractive candidate for Na-ion batteries. Besides, as the ionic radius of Na^+ (ionic radius 1.02 Å) is bigger than that of 3d metal cations, the chances of NaNMC having intersites mixing between Ni^{2+} and Na^+ ion upon cycling is limited, as compared to the LiNMC electrode owing to the fact that Ni^{2+} (0.69 Å) and Li^+ (0.76 Å) have closer ionic radii.[17,18] For such reasons we decided to revisit the Na-based layered oxides with special attention to the Na-$Ni_{1/3}Mn_{1/3}Co_{1/3}O_2$ (denoted hereafter NaNMC) for which we report its synthesis, structure, and electrochemical properties. The insertion of Na into this phase, which shows a sustained reversible capacity of 120 mAh·g^{-1}, is found to drive several structural phase transitions that we have studied by *in situ* X-ray diffraction.

Received: February 11, 2012
Revised: April 16, 2012
Published: April 17, 2012

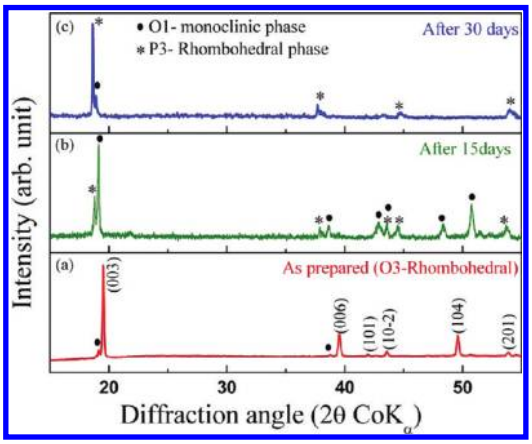

Figure 1. Powder X-ray diffraction pattern demonstrating structural stability of $NaNi_{1/3}Mn_{1/3}Co_{1/3}O_2$ on exposure to air: (a) as-prepared $NaNi_{1/3}Mn_{1/3}Co_{1/3}O_2$ (rhombohedral; O3 phase), (b) $NaNi_{1/3}Mn_{1/3}Co_{1/3}O_2$ after 15 days of exposure to air (monoclinic O1 phase), and (c) $NaNi_{1/3}Mn_{1/3}Co_{1/3}O_2$ after 30 days of exposure to air (rhombohedral; P3 phase).

EXPERIMENTAL SECTION

Layered NaNMC with nominal stoichiometry of $NaNi^1/_3Mn^1/_3Co^1/_3O_2$ was prepared by the sol−gel method using acetate of Na, Co, Ni, and Mn in the molar ratio 1.05:0.33:0.33:0.33 and citric acid as chelating agent, respectively. The aqueous solution of the resulting precursor complex was heated on a hot plate at 80 °C under constant stirring to obtain a gel that upon further heating to 400 °C decomposed to yield a homogeneously mixed amorphous powder containing carbon residues. The obtained decomposition product was heated in a muffle furnace at 900 °C for 12 h, slowly cooled (1 °C/min) to 300 °C, removed from the furnace and transferred into an inert atmosphere glovebox where it was ground and stored to avoid any reaction with moisture and carbon dioxide.

Characterization. Powder X-ray Diffraction (XRD) pattern of the synthesized sample was recorded with a Philips X'pertPro diffractometer (Co K_α, λ=1.78897 Å). The lattice parameters were determined using the refinement software, General Structure Analysis System (GSAS) code.[19] The morphological studies were carried out with an Hitachi (Model S-3000 H) scanning electron microscope with EDX facility for elemental analysis. The stoichiometry of metal atoms in the sample was determined by atomic absorption spectroscopy (AAS, Perkin-Elmer Analyst 100) after dissolution of a known amount of sample in a $H_2O/H_2O_2/HNO_3$ (90/7/3 v/v/v) solution.

Positive electrodes were prepared by mixing 85 wt % of active material with 15 wt % of SP carbon, as electronic conductor. Swagelok-type cells were assembled in an argon filled glovebox with about 10 mg of the carbon/material mix separated from the negative electrode (sodium metal disk pressed on a stainless steel current collector) by 3 sheets of glass fiber disks, which are soaked with a 1 M solution of $NaClO_4$ in an ethylene carbonate (EC)/dimethyl carbonate (DMC) mixture (1/1 v/v). At this stage, $NaClO_4$ being a strong oxidizer, care should be taken in handling it. Galvanostatic charge/discharge cycles were conducted at constant temperature (30 °C) on Na half cells with a voltage between 2.0−3.75 V using the VMP3 (Biologic) multichannel potentiostat/galvanostat. The charge discharge studies were carried out at a rate of 1 Na per formula unit in 10 h (denoted as C/10) which corresponds to a current of ~0.24 mA·cm^{-2}. In a typical experiment, the current density during galvanostatic cycling is maintained constant for both charge and discharge. The electrochemically driven structural evolution of the electrode materials during Na insertion/deinsertion reaction was monitored by *in situ* XRD using D-8 Bruker diffractometer (CoK$_\alpha$, λ = 1.78897 Å, Position Sensitive Detector) and a specially designed Swagelok cell equipped with an

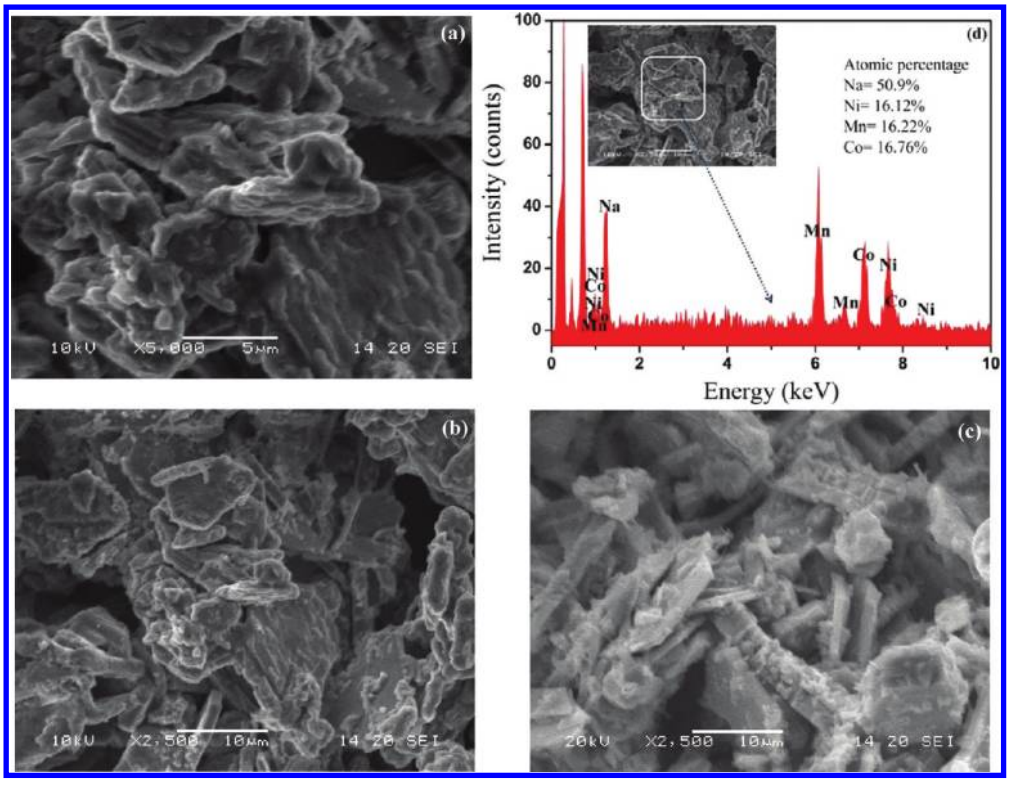

Figure 2. Scanning electron microscopic images of (a) as-prepared $NaNi^1/_3Mn^1/_3Co^1/_3O_2$, (b) $NaNi^1/_3Mn^1/_3Co^1/_3O_2$ after 15 days air exposure, (c) $NaNi^1/_3Mn^1/_3Co^1/_3O_2$ after 30 days air exposure, and (d) EDAX spectrum showing the composition of various elements in the NaNMC. Atomic ratio of the elements are Na:Ni:Mn:Co = 1.03:0.33:0.33:0.33.

dx.doi.org/10.1021/cm300466b | *Chem. Mater.* 2012, 24, 1846−1853

X-ray-transparent beryllium window acting as current collector.[20] The *in situ* XRD patterns were collected along charge or discharge recorded at a C/20 rate (1 Na in 20 h which corresponds to a current ~0.12 mA·cm^{-2}).

RESULTS AND DISCUSSION

The powder X-ray diffraction (XRD) of NaNMC shown in Figure 1(a) indicated the absence of impurity phases corresponding to cobalt, nickel, or manganese oxides and sodium salts. The pattern could be indexed with the Na_xCoO_2 model structure with rhombohedral symmetry ($R\bar{3}m$) (PDF No: 01-070-2030). However, we observe weak additional peaks marked with '•' which corresponds to the onset of a second phase crystallizing in the monoclinic $C2/m$ space group (PDF No: 00-032-1068). This structural transition from rhombohedral to monoclinic and vice versa is well-known[21] to be associated with the gliding of $(Ni_{0.33}Mn_{0.33}Co_{0.33}O_2)_n$ slabs with respect to each other and usually due to changes in alkali content. To explore further the origin of the monoclinic phase, we checked the stability of samples when aged in air. The NaNMC samples were exposed to air for several days, and XRDs were recorded at regular intervals. Typical patterns after exposure to 15 days and 30 days are shown in Figure 1(b) and Figure 1(c).

They indicate several new reflections which are not present in the case of the rhombohedral phase. Besides, peaks corresponding to (006) and (104) reflections, which are specific to a rhombohedral phase, are absent in the pattern shown in Figure 1(b). The new reflections could be matched with those of the monoclinic O1 phase and the P3-type rhombohedral phase typically observed for nonstoichiometric phases like $Na_{0.6}CoO_2$. We presume here that the structural transformation of NaNMC from rhombohedral O3 to monoclinic O1-type and to rhombohedral P3-type is triggered by reactions with H_2O and CO_2 on exposure to air (eq 1), which results in nonstoichiometric $Na_{(1-x)}$NMC samples.

$$NaNi_{0.33}Mn_{0.33}Co_{0.33}O_2 + CO_2/OH \rightarrow Na_{1-x}Ni_{0.33}Mn_{0.33}Co_{0.33}O_2 + x\text{NaOH or } x/2\ Na_2CO_3 \quad (1)$$

The IR spectrum recorded on exposed sample revealed the presence of IR bands corresponding to CO_3^{2-} and OH bending and stretching modes. The bands at 3407 cm^{-1} are attributed to ν (O−H) and those at 1630 cm^{-1} to δ (O−H). Those appearing at 1450 cm^{-1} ν (C−O) and 863 cm^{-1} to δ (OCO) are due to carbonates (see Supporting Information, S-1). This confirms the partial conversion of Na to Na_2CO_3/NaOH. The sodium partial departure from NaNMC results in the sliding of $(Ni_{0.33}Mn_{0.33}Co_{0.33}O_2)$ layers, which in turn drive the sodium from an octahedral environment to a prismatic position. In general, the layered phases are denoted as O3, O1, P3, and P1 phases.[22,23] The letter O and P represent Na in octahedral and prismatic environments, respectively. The numbers 3 or 1 represent the number of MO_2 layers per unit cell.

The microstructure of the sample was investigated using scanning electron microscopy. Typical SEM image of as-prepared NaNMC shown in Figure 2(a) indicate agglomeration of flaky particles with sizes ranging between 1 and 10 μm. EDX analysis has been carried out on several particles, and the characteristic EDX spectrum is shown in Figure 2(d). The composition as deduced from the EDX analysis is

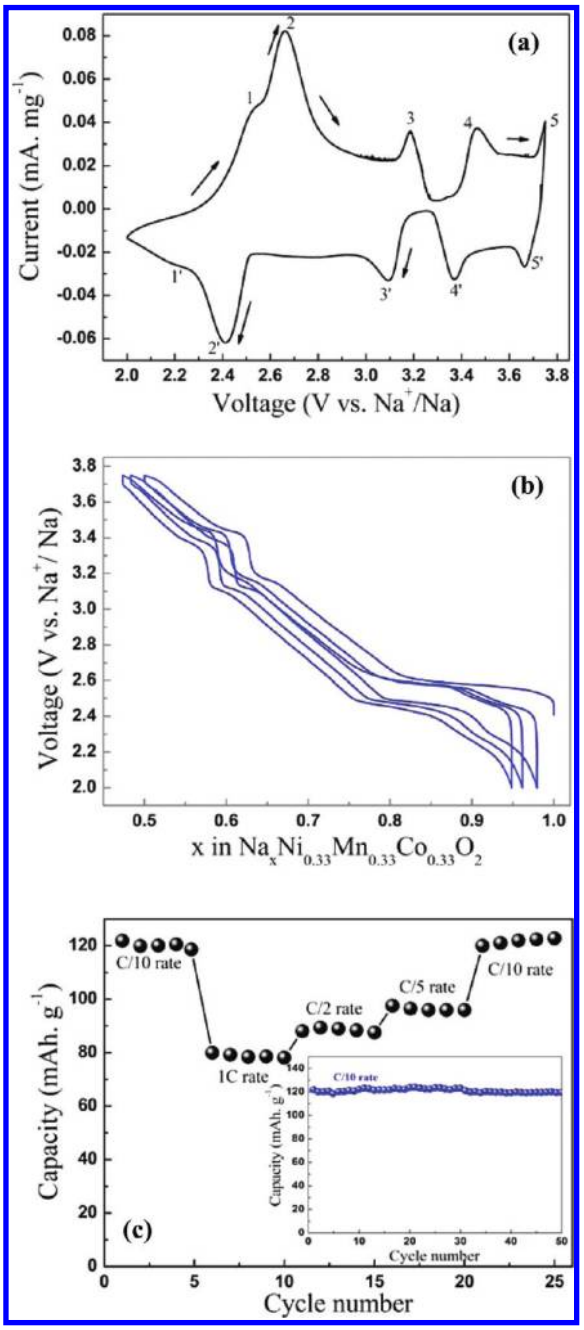

Figure 3. (a) Cyclic voltammogram of $NaNi^{1}/_{3}Mn^{1}/_{3}Co^{1}/_{3}O_2$ at a scan rate of 0.1 mV/s between 2 to 3.75 V. (b) Voltage vs composition profile of $NaNi^{1}/_{3}Mn^{1}/_{3}Co^{1}/_{3}O_2$ as deduced from galvanostatic cycling at 0.1C rate. (c) Rate capability plot showing cycling performance at various rates. Inset of (c) shows plot of capacity retention with respect to cycle numbers.

$Na_{1.03}Ni_{0.33}Mn_{0.33}Co_{0.33}O_2$, in agreement with the nominal composition of NaNMC, which was confirmed by elemental analysis using atomic absorption spectroscopy. For comparison, SEM images of NaNMC after being exposed to air for 15 and 30 days are shown in Figure 2(b) and 2(c), respectively. No noticeable changes appear for the 15 days exposed sample. This contrasts with the SEM images collected on 30 days exposed samples which show the growth of Na_2CO_3 segregated over the entire sample surface.

The electrochemical performance of NaNMC was evaluated using sodium half cells. The NaNMC/Na cell showed an open

dx.doi.org/10.1021/cm300466b | *Chem. Mater.* 2012, 24, 1846−1853

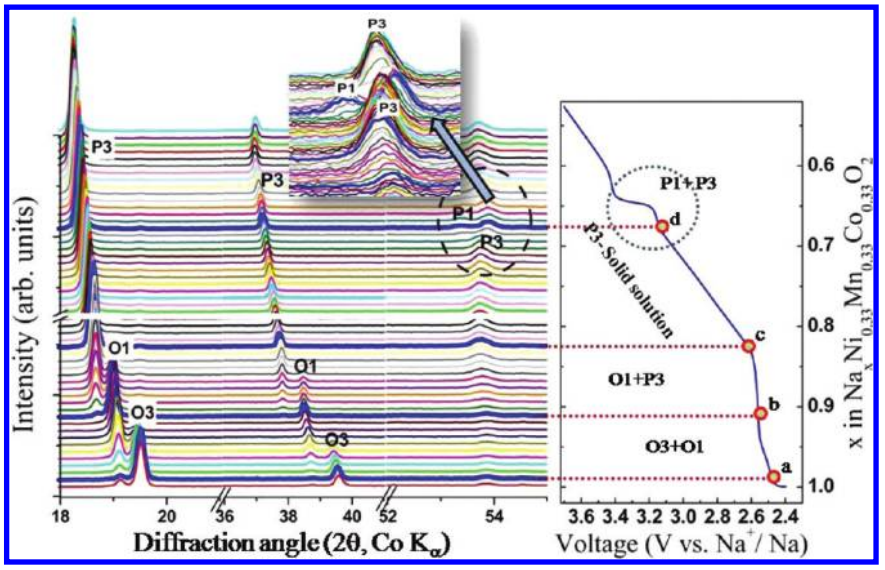

Figure 4. *In situ* X-ray diffraction patterns collected during the first charge (up to 3.7 V at C/20 rate) for a $NaNi_{1/3}Mn_{1/3}Co_{1/3}O_2$ vs Na cell. Corresponding voltage-composition profile is given on the right side. The diffraction angle of 15 to 55 was used for the *in situ* studies; however, for clarity the uninteresting regions are not mentioned. The inset of the figure shows an enlarged portion of the high angle region.

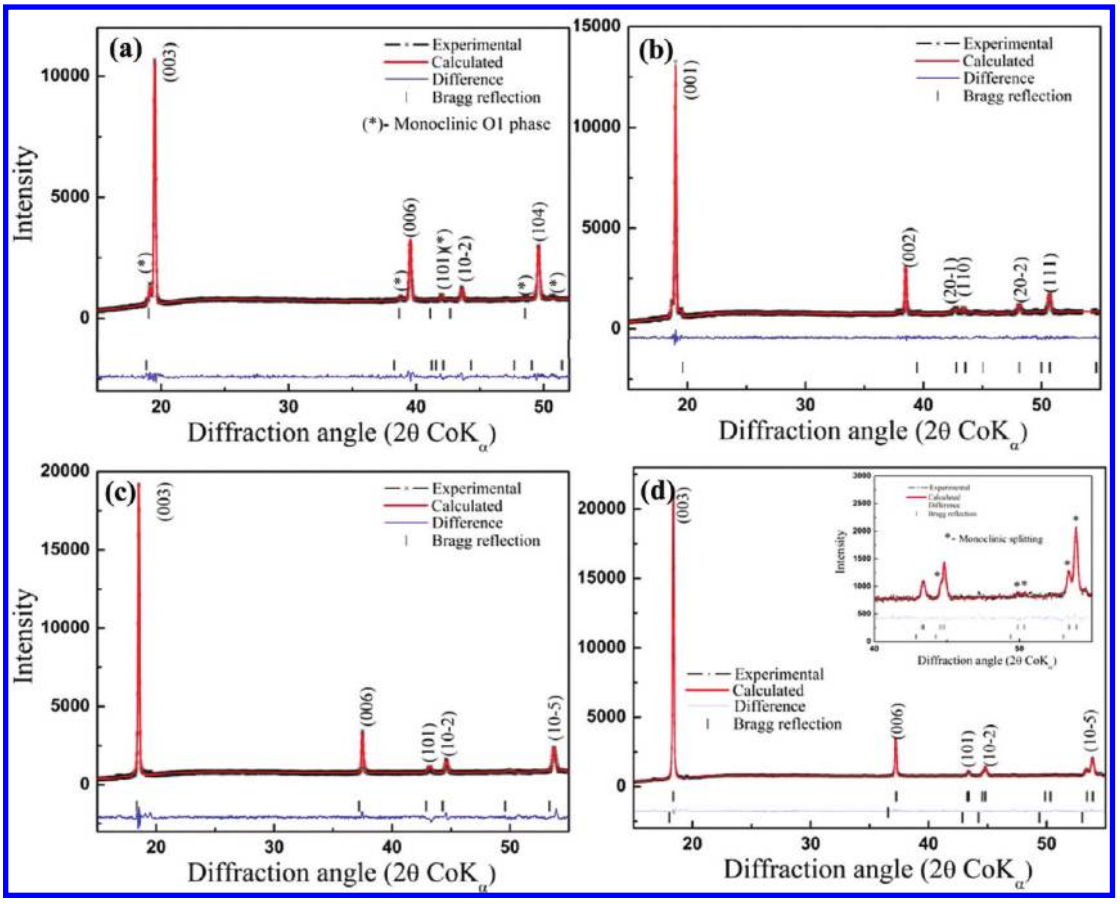

Figure 5. Powder XRD Rietveld fit for the distinct phase of $Na_xNi^{1}{}_{/3}Mn^{1}{}_{/3}Co^{1}{}_{/3}O_2$ that evolved during electrochemical *in situ* studies. (a) Powder XRD Rietveld fit for the initial phase $NaNi^{1}{}_{/3}Mn^{1}{}_{/3}Co^{1}{}_{/3}O_2$. Refinement had been carried out using two phases with phase fractions: 90% rhombohedral phase and 10% monoclinic phase (marked *). (b) Rietveld fit for the monoclinic O1 phase, observed for composition of $Na_{0.9}Ni^{1}{}_{/3}Mn^{1}{}_{/3}Co^{1}{}_{/3}O_2$ (2.58 V). (c) Rietveld fit for the rhombohedral P3 phase, observed for composition of $Na_{0.83}Ni^{1}{}_{/3}Mn^{1}{}_{/3}Co^{1}{}_{/3}O_2$ (2.62 V). (d) Rietveld fit for the monoclinic P1 phase, observed for composition of $Na_{0.67}Ni^{1}{}_{/3}Mn^{1}{}_{/3}Co^{1}{}_{/3}O_2$ (3.16 V).

circuit potential of 2.4 V which is below the reduction potential of water (3.94 V vs Na/Na^+). It does not come as a surprise then that NaNMC samples react with moisture when aged in air. Figure 3(a) shows the second cyclic voltammogram of

dx.doi.org/10.1021/cm300466b | *Chem. Mater.* 2012, 24, 1846–1853

Table 1. Refined Crystallographic Parameters Obtained with Distinct Phases Observed during Electrochemical *in situ* X-ray Diffraction

(i) O3-Rhombohedral $NaNi_{0.33}Mn_{0.33}Co_{0.33}O_2$[a]					
atom	Wyckoff position	x	y	z	occupancy
Na	3b	0.0	0.0	0.0	1.00
Ni/Mn/Co	3a	0.0	0.0	0.5	0.33
O	6c	0.0	0.0	0.2407(1)	1.00
(ii) O1-Monoclinic $Na_{0.9}Ni_{0.33}Mn_{0.33}Co_{0.33}O_2$[b]					
atom	Wyckoff position	x	y	z	occupancy
Na	2d	0.0	0.5	0.5	0.9
Ni/Mn/Co	2a	0.0	0.0	0.0	0.33
O	4i	0.2394(2)	0.0	0.7747(0)	1.00
(iii) P3-Rhombohedral $Na_{0.8}Ni_{0.33}Mn_{0.33}Co_{0.33}O_2$[c]					
atom	Wyckoff position	x	y	z	occupancy
Na	3a	0.0	0.0	0.1773(6)	0.8
Ni/Mn/Co	3a	0.0	0.0	0.0	0.33
O1	3a	0.0	0.0	0.4007(7)	0.5
O2	3a	0.0	0.0	0.574062	0.5
(iv) P1-Monoclinic $Na_{0.65}Ni_{0.33}Mn_{0.33}Co_{0.33}O_2$[d]					
atom	Wyckoff position	x	y	z	occupancy
Na	4i	0.806	0.0	0.4912(4)	0.33
Ni/Mn/Co	2a	0.0	0.0	0.0	0.33
O1	4i	0.3871(7)	0.0	0.1743(4)	1.00

[a]Lattice parameters: a = 2.9624(7) Å, b = 2.9624(7) Å, c = 16.1020(6) Å; α = 90, β = 90, γ = 120; space group: R$\bar{3}$m; R_{wp}= 4.35, χ^2 = 1.55. [b]Lattice parameters: a = 5.0229(5) Å, b = 2.9420(8) Å, c = 5.8907(2) Å; α = 90, β = 111.3886, γ = 90; space group: C2/m; R_{wp}= 3.33, χ^2 = 1.42. [c]Lattice parameters: a = 2.8479(6) Å, b = 2.8479(6) Å, c = 16.6093(3) Å; α = 90, β = 90, γ = 120; space group: R3m; R_{wp}= 4.27, χ^2 = 1.511. [d]Lattice parameters: a = 5.0151(4) Å, b = 2.7707(9) Å, c = 5.9338(1) Å; α = 90, β = 108.2027, γ = 90; space group: C2/m; R_{wp}= 4.58, χ^2 = 1.402.

$NaNi^{1}/_{3}Mn^{1}/_{3}Co^{1}/_{3}O_2$ vs Na cells in the voltage range of 2−3.75 V at a scan rate of 0.1 mV/s. It shows five current peaks at 2.53, 2.66, 3.19, 3.46, and 3.74 V in the anodic sweep and five peaks as well (2.21, 2.41, 3.09, 3.37, and 3.66 V) in the cathodic scan indicative of a reversible sodium insertion-deinsertion process.

The voltage vs composition curve for NaNMC (Figure 3(b)) shows both in discharge and charge a stairlike profile indicative of a reversible Na-driven structural transition. Note that within the 2−3.75 V voltage window, 0.5 Na^+ per mole of NaNMC can be removed upon oxidation and uptake during the subsequent reduction. This leads to an overall reversible capacity of 120 mAh·g^{-1}. Interestingly, the voltage composition profile (Figure 3(b)) is identical to that reported for $NaNi_{1/2}Mn_{1/2}O_2$ wherein the capacity originates from the $Ni^{2+} \Leftrightarrow Ni^{4+}$ redox couple.[14] This seems to indicate that, within the explored potential window, the measured capacity for NaNMC originates from the Ni^{4+}/Ni^{2+} redox couple as well. Further, pursuing comparisons, we should recall that the high capacity of 220 mAh·g^{-1} measured for LiNMC between 2.75 to 4.2 V, and which corresponds to the removal of 0.8 Li^+, has been ascribed to the sequential oxidation of 0.33 mols of $Ni^{2+} \rightarrow Ni^{3+} \rightarrow Ni^{4+}$ accounting to 0.66 Li^+, with the removal of the last 0.14 Li^+ due to the partial oxidation of Co^{3+} to Co^{4+}. Although we have not done *in situ* XANES measurements to monitor Ni^{2+} variation, one belief from the aforementioned comparisons that the capacity measured for NaNMC below 3.7 V and corresponding to 0.5 Na^+ is due to the partial oxidation of Ni^{2+} into Ni^{3+} and Ni^{4+}. The main difference between both systems, except for the structure, resides in the fact that we could not utilize the remaining 0.16 Na^+ owing to copious electrolyte decomposition (see Supporting Information, S-2 with namely an irreversible plateau region above 4 V).

The rate capability performances of NaNMC electrodes galvanostatically cycled in the voltage range of 2.0 to 3.75 V are shown in Figure 3(c). It demonstrates the feasibility of solely achieving 75% of the initial capacity at 1C rate, which is indicative of a slow kinetic Na insertion-deinsertion process. The inset of Figure 3(c) shows the capacity retention plot as a function of the number of cycles at 0.1C rate for a NaNMC electrode.

The initial capacity of 120 mAh·g^{-1} is retained without much loss even after 50 cycles when the cell is operated over the 2.5−3.75 V voltage window. Higher capacity values >120 mAh·g^{-1} can be reached when raising the charge cut off voltage to 4.2 V but to the expense of intense capacity loss during the first few cycles. There are several possible reasons to account for such capacity loss. Among them are the increasing catalytic decomposition of the Na-based electrolyte with increasing the charging voltage and the increasing irreversibility of the electrode material associated to Na-driven structural changes.[14]

In order to grasp some insight in the Na intercalation/deintercalation mechanism and more specifically in the Na-driven structural transformation, *in situ* X-ray diffraction was recorded during the first charge (up to 3.7 V). Figure 4 shows the *in situ* X-ray diffraction patterns recorded during the first charge of a $NaNi^{1}/_{3}Mn^{1}/_{3}Co^{1}/_{3}O_2$ electrode. It unveils a phase evolution during sodium deintercalation. The *in situ* XRD profile shows that the initial phase is O3-type rhombohedral with a small amount of O1-type monoclinic phase (which origin was discussed in the previous section). The peak at 19.58° corresponds to (003) reflection of the O3-type phase.[24] On the other hand, the peak at 19.13° corresponds to the (001) reflection of the monoclinic phase. The intensity of reflections corresponding to the O3 phase at 2θ = 19.58° and 39.5° decreases with an increase in the intensity of the peaks at 2θ = 19.13° and 39.2° indicating the transformation of the O3 phase into a O1 phase for a small region of 'x'; $1 < x < 0.9$. The complete transformation of Na_xNMC to monoclinic (O1-type) is observed at x = 0.9 (the region represented as 'b' in the voltage-composition profile, Figure 4). Such a monoclinic distortion is the result of a gliding of oxygen planes associated with Na removal. It can be indexed as either O1 type (reduced unit cell) or O'3 if superstructure peaks can be seen in the X-ray powder pattern as reported in the literature. Presently no extra superstructures peaks could be spotted in our XRD pattern collected from Lab X-ray sources, the reason why we have indexed our phase as O1 type. We therefore recognize that synchrotron experiments, as planned, are sorely needed to clarify this structural point. On further deintercalation of Na, the intensity of the O1 phase decreases as the intensity of the P3 (rhombohedral) phase increases, indicating another biphasic domain (O1+P3) corresponding to a value of $0.9 < x < 0.82$. The concentration of the P3 phase increased as the x value approaches 0.83, and at x = 0.83 a P3-type single phase is observed. In the P3 phase, Na is in trigonal prismatic coordination which is simply caused by the $MO_2^{\delta-}$ layers becoming less negatively charged so that the trigonal prismatic environment is favored over the octahedral one. The region representing the P3

dx.doi.org/10.1021/cm300466b | *Chem. Mater.* 2012, 24, 1846−1853

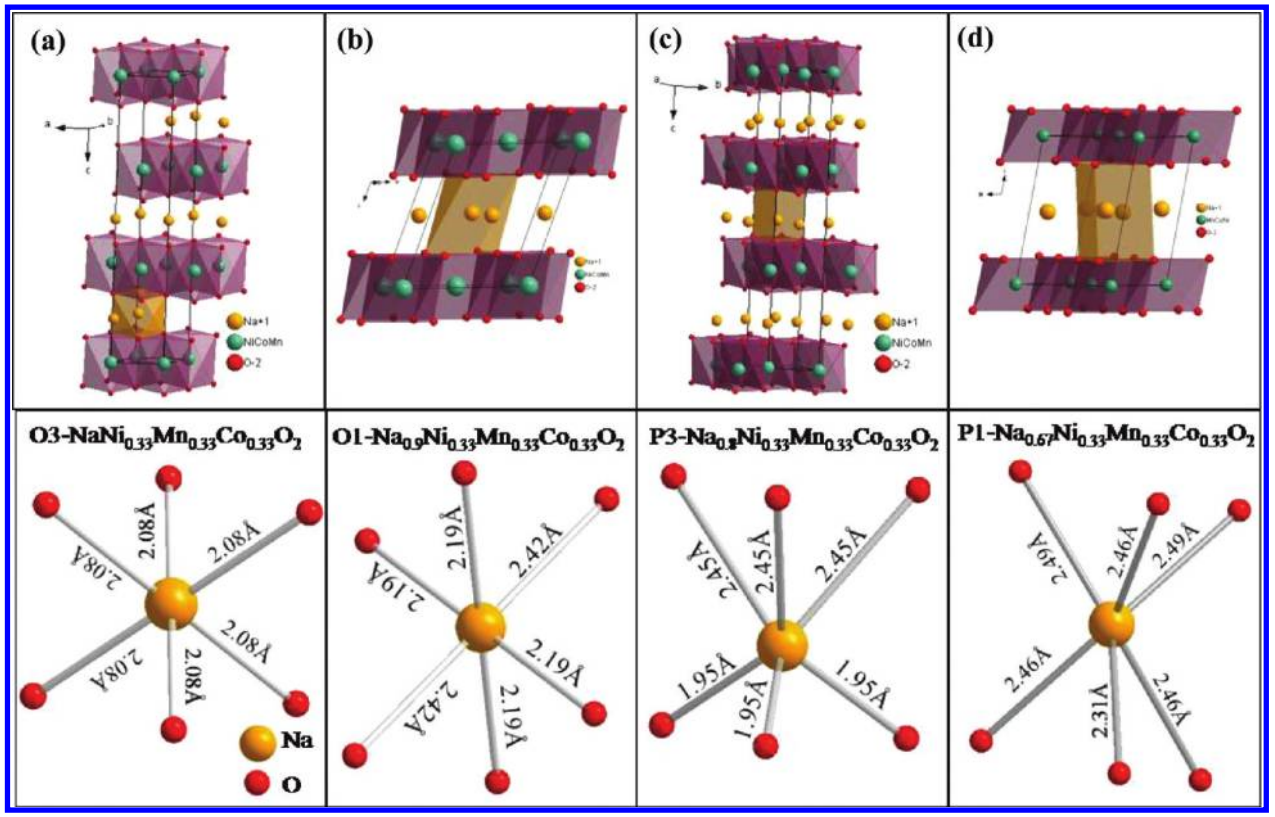

Figure 6. Crystal structure of $Na_xNi^1_{/3}Mn^1_{/3}Co^1_{/3}O_2$ and the corresponding NaO_6 coordination polyhedra. The bond length for each of Na−O is given in the lower panel. (a) The O3 phase represents Na in octahedral geometry with three MO_2 layers per unit cell. (b) The O1 phase represents Na in octahedral geometry with one single MO_2 layer. (c) P3 represents Na in prismatic geometry with three MO_2 layers. (d) P1 represents Na in prismatic geometry with one single MO_2 layer.

phase is shown as 'c' in the voltage-composition profile (Figure 4), and the corresponding XRD is represented by a thick line. On further deintercalation of Na until x = 0.67, a monophasic solid solution of P3-type is observed. At x = 0.67, the monoclinic splitting of the peak at 54° is observed, which corresponds to the (10−5) reflection of the P1 phase. The enlarged image of the region is shown as inset. The small biphasic region P1+P3 is observed for the x value of 0.67 < x <0.6; at x = 0.6 and below, the solid solution of P3-type is observed. This P3-type phase which corresponds to a tripling of the P1 unit cell is then preserved to higher potentials.

Rietveld refinements were carried out using GSAS Rietveld suite,[19] and the results are reported in Figure 5(a-d) for the O3, O1, P3, and P1 crystallographic phases, respectively. The refinement for the initial phase (Figure 5(a)) was best converged with a two-phase refinement having 90% of rhombohedral (O3) and 10% of monoclinic (O1) phase. However, monophasic regions represented as 'b', 'c', and 'd' on the voltage-composition profile (Figure 4) of the *in situ* cell correspond to O1-, P3-, and P1-phases observed for compositions such as $Na_{0.9}Ni^1_{/3}Mn^1_{/3}Co^1_{/3}O_2$ (potential of 2.58 V), $Na_{0.83}Ni^1_{/3}$-$Mn^1_{/3}Co^1_{/3}O_2$ (potential of 2.62 V), and $Na_{0.67}Ni^1_{/3}Mn^1_{/3}Co^1_{/3}O_2$ (potential of 3.16 V), respectively. The crystallographic data and the refined parameters for the above phases are given in Table 1. The structure of rhombohedral and monoclinic phases represented as O3, O1, P3, and P1 are shown in Figure 6(a-d), respectively.

The rhombohedral O3 structure consists of layers of edge-sharing MO_6 octahedra separated by Na ions with three MO_2 layers per unit cell. Na deintercalation from rhombohedral $NaNi^1_{/3}Mn^1_{/3}Co^1_{/3}O_2$ resulted in the repulsion of MO_2 layers causing the expansion and distortion of NaO_6 octahedra. The increased bond length (compared to the O3 phase) is shown in the lower panel of Figure 6(b). Na deintercalation beyond $Na_{0.9}Ni^1_{/3}Mn^1_{/3}Co^1_{/3}O_2$ resulted in further expansion of MO_2 layers forcing NaO_6 to take a prismatic environment for the P3 and P1 phases[23] Figure 6(c) and (d).

The evolution of the '*a*' and '*c*' cell parameters during the electrochemical removal of Na from $Na_xNi^1_{/3}Mn^1_{/3}Co^1_{/3}O_2$, as deduced from *in situ* XRD measurements, is shown in Figure 7. We have used the conversion relation between hexagonal and monoclinic lattice, $a_{hex} = a_{mon}/\sqrt{3}$; $b_{hex} = b_{mon}$; $c_{hex} = 3c_{mon}\sin\beta$ so as to obtain comparative values.[12] The '*c*' lattice parameter increases with decreasing the Na content. This indicates an increase in repulsion between alternate MO_2 layers which is consistent with the lower screening effect exerted by the Na ions as they are removed from the van der Waals gap. It should be noted here that the '*c*' parameter remains constant for the biphasic regions as the concentration of the first phase decreases with an increase in concentration of the second phase (it is also evident from the increase and decrease in intensity corresponding to two phases in the *in situ* XRD profile).

However, for the solid solution domain the *c*-parameter keeps increasing. In contrast, the '*a*'-lattice parameter slightly decreases with decreasing the sodium content, and this can simply be explained by a reduction in size of the Ni 3d-metal upon its oxidation.

Besides their attractive electrochemical properties, Na-based cobalt oxide systems can present attractive physical properties. For

dx.doi.org/10.1021/cm300466b | *Chem. Mater.* 2012, 24, 1846−1853

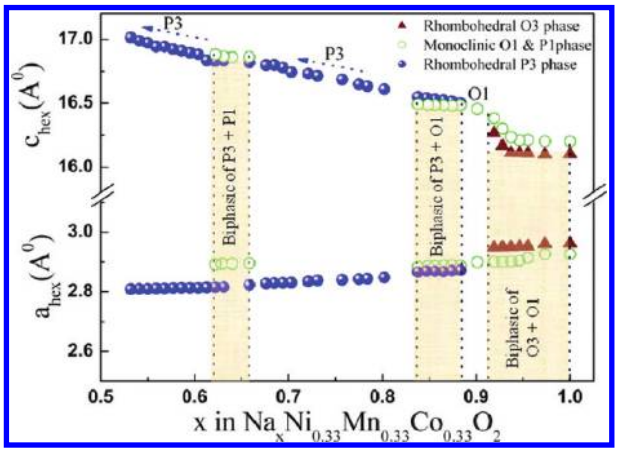

Figure 7. Evolution of cell parameters ('*a*' and '*c*') as a function of Na concentration and the phases in the $Na_xNi^{1}/_{3}Mn^{1}/_{3}Co^{1}/_{3}O_2$ system during an electrochemical charge on NaNMC vs Na *in situ* cell. To understand the trend of variation in c_{hex} and a_{hex} parameters as a function of *x*, relation, $a_{hex} = a_{mon}/\sqrt{3}$; $b_{hex} = b_{mon}$; $c_{hex} = 3c_{mon}\sin\beta$ is used for calculation.

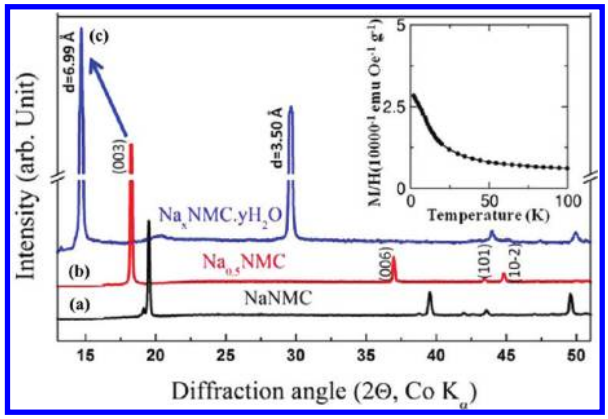

Figure 8. X-ray diffraction pattern of (a) NaNMC and (b) Na_xNMC charged up to 3.75 V ($x = 0.5$) and (c) Na_xNMC treated with water, ($Na_xNMC{\cdot}yH_2O$). The inset of the figure shows magnetization data.

instance, way back in 2003, Takada et al.[25] showed the feasibility of preparing a superconducting phase of composition $Na_{0.35}CoO_2{\cdot}1.3H_2O$ having a CdI_2 structure similar to that of CoO_2 with a superconducting temperature Tc of 5 K. The synthesis was carried out through the removal of 0.35 Na atoms from the layered $Na_{0.7}CoO_2$ by a chemical oxidation in the presence of Br_2 followed with an uptake of H_2O molecules. In this context it was tempting to search for superconductivity in our Na-NMC phases, and therefore we exposed our electrochemically oxidized Na_xNMC to water and noted a rapid change in the XRD powder pattern, as shown in Figure 8. For reasons of clarity, we are just reporting the X-ray diffraction patterns of the as-made NaNMC phase; that of $Na_{0.5}NMC$ obtained by charging to 3.75 V together with that of the $Na_{0.5}NMC{\cdot}H_2O$ obtained by treating $Na_{0.5}NMC$ with water are depicted in Figure 8.

The shift in the (003) Bragg peak position to low angle indicates an increase in the lattice spacing associated to the intercalation of water molecules. This was confirmed by TGA measurements coupled with mass spectrometry, which indicate an uptake of one water molecule per unit formula. The newly formed phase, $Na_{0.5}NMC{\cdot}H_2O$, having the following lattice parameters, $a = 2.676$ Å, $c = 21.00$ Å, was checked for superconductivity using a superconducting quantum interference device magnetometer (SQUID). The temperature dependence of the magnetic susceptibility down to 4K reveals a paramagnetic behavior (inset of Figure 8) with the absence of any magnetic ordering or superconducting transition temperature irrespective of the composition of $Na_xNMC{\cdot}nH_2O$ samples we have tried.

CONCLUSIONS

In summary, we have prepared a new layered Na compound, NaNMC analogous to LiNMC. This Na-based phase, which shows a capacity of 120 mAh·g^{-1} corresponding to the reversible insertion of 0.5 Na below 3.75 V and exhibits good capacity retention, stands as an attractive positive electrode for sodium ion battery provided we could improve its rate capability. Its voltage profile shows a stairlike variation with each step associated to the formation of distinct phases O3, O1, P3, and P1 which differ from each other by a specific gliding of the oxides layers. Finally, we demonstrated that NaNMC is air unstable and long exposure results in a nonstoichiometric $Na_xNMC{\cdot}H_2O$ hydrated phase which did not show superconductivity at low temperature unlike the $Na_{0.35}CoO_2{\cdot}1.3H_2O$ phase. Further work is being presently pursued toward the design of electrolytes highly resistant against oxidation so that we can increase the charge cut off cell voltage and therefore the electrode energy density.

ASSOCIATED CONTENT

Supporting Information

Figures S-1−S-3. This material is available free of charge via the Internet at http://pubs.acs.org.

AUTHOR INFORMATION

Corresponding Author

*E-mail: prakash.as@gmail.com.

Notes

The authors declare no competing financial interest.

ACKNOWLEDGMENTS

This work was supported by the Council of Scientific and Industrial Research, New Delhi, India under EMPOWER grant scheme (DU-01 OLP-0062) and CSIR-NISE (CECRI NWP-56B, TAPSUN programme). Ms. M. Sathiya thanks the CSIR, New Delhi for granting Fellowship. Special thanks to Prof A. K. Shukla, (IISc, Bangalore) for helpful discussions and technical support. Thanks are due to B. Melot (University of Picardie) and J. Neilson (Johns Hopkins University) for conducting the magnetic measurements.

REFERENCES

(1) Tarascon, J.-M.; Armand, M. *Nature* **2001**, *414*, 359−367.
(2) Palacin, M. R. *Chem. Soc. Rev* **2009**, *38*, 2565−2575.
(3) Tarascon, J.-M. *Nat. Chem.* **2010**, *2*, 510−510.
(4) Armand, M.; Tarascon, J.-M. *Nature* **2008**, *451*, 652−657.
(5) Doeff, M. M.; Visco, S. J.; Ma, Y.; Peng, M.; Ding, L.; D-Jonghe, L. C. *Electrochim. Acta* **1995**, *40*, 2205−2209.
(6) Berthelot, R.; Carlier, D.; Delmas, C. *Nat. Mater.* **2011**, *10*, 74−80.
(7) Delmas, C.; Braconnier, J- J.; Fouassier, C.; Hagenmuller, P. *Solid State Ionics* **1981**, *3/4*, 165−169.
(8) Sauvage, F.; Laffont, L.; Tarascon, J.-M.; Baudrin, E. *Inorg. Chem.* **2007**, *46*, 3289−3294.

(9) Ma, X.; Chen, H.; Ceder, G. *J. Electrochem. Soc.* **2011**, *158* (12), A1307−A1312.
(10) Delmas, C.; Borthomieu, Y.; Faure, C. *Solid State Ionics* **1989**, *32/33*, 104−111.
(11) Abraham, K. M. *Solid State Ionics* **1982**, *7*, 199−212.
(12) Saadoune, I.; Maazaz, A.; Menetrier, M.; Delmas, C. *J. Solid State Chem.* **1996**, *122*, 111−117.
(13) Lu, Z.; Dahn, J. R. *J. Electrochem. Soc.* **2001**, *148* (11), A1225−1229.
(14) Komaba, S.; Nakayama, T.; Ogata, A.; Shimizu, T.; Takei, C.; Takada, S.; Hokura, A.; Nakai, I. *ECS Trans.* **2009**, *16* (42), 43−55.
(15) Ohzuku, T.; Makimura, Y. *Chem. Lett.* **2001**, *30*, 642.
(16) Sathiya, M.; Prakash, A. S.; Ramesha, K.; Shukla, A. K. *Mater. Res. Bull.* **2009**, *44*, 1990−1994.
(17) Hirano, A.; Kanno, R.; Kawamoto, Y.; Takeda, Y.; Yamaura, K.; Takana, M.; Ohyama, K.; Ohashi, M.; Yamaguchi, Y. *Solid State Ionics* **1995**, *78*, 123−131.
(18) Kang, K.; Meng, Y. S.; Breger, J.; Grey, C. P.; Ceder, G. *Science* **2006**, *311*, 977−980.
(19) Larson, A. C.; R. B. Van Dreele, R. B. Los Alamos National Laboratory Report No. LAUR 86- 748; 2000. Toby, B. H. *J. Appl. Crystallogr.* **2001**, *34*, 210.
(20) Prakash, A. S.; Larcher, D.; Morcrette, M.; Hegde, M. S.; Leriche, J.-B.; Masquelier, C. *Chem. Mater.* **2005**, *17*, 4406−4415.
(21) Hamani, D.; Ati, M.; Tarascon, J.-M.; Rozier, P. *Electrochem. Commun.* **2011**, *13*, 938−941.
(22) Delmas, C.; Fouassier, C.; Hagenmuller, P. *Physica* **1980**, *99B*, 81−85.
(23) Szajwaj, O.; Gaudin, E.; Weill, F.; Darriet, J.; Delmas, C. *Inorg. Chem.* **2009**, *48*, 9147−9154.
(24) Viciu, L.; Bos, J. W. G.; Zandbergen, H. W.; Huang, Q.; Foo, M. L.; Ishiwata, S.; Ramirez, A. P.; Lee, M.; Ong, N. P.; Cava, R. J. *Phys. Rev. B* **2006**, *73*, 174104 (1−10).
(25) Takada, K.; Sakurai, H.; Muromachi, E. T-; Izumi, F.; Dilanian, R. A.; Sasaki, T. *Nature* **2003**, *422*, 53−55.